JOURNAL OF MATERIALS SCIENCE 22 (1987) 3873–3879

Effect of residual stress on crack propagation in MDPE pipes

K. CHAOUI, A. CHUDNOVSKY, A. MOET*
*Department of Civil Engineering, and *Department of Macromolecular Science, Case Western Reserve University, Cleveland, Ohio 44106, USA*

Crack propagation behaviour in single edge notched specimens prepared from medium-density polyethylene (MDPE) pipe is examined under creep condition. The crack grown from an exterior notch (inbound) initiated faster than that grown from an interior notch (outbound). Subsequently, the outbound crack propagated monotonically to ultimate failure. The inbound crack showed anomalous behaviour involving two arrest stages prior to ultimate failure. The pipe is found to possess substantial residual stresses. The energy release rate for each case was calculated taking into account the respective residual stress distribution. The fact that the rates of crack propagation are not a unique function of the energy release rate indicates that the fracture is also influenced by morphological gradients imposed by processing conditions.

1. Introduction

Residual stresses in plastic pipes are a consequence of the thermomechanical history imparted by extrusion. Different cooling rates on the inner and outer surfaces of the pipe wall create a gradient of temperature [1] which results in residual stresses and morphological differences [2–4]. Similar effects may also arise from the non-homogeneity of melt flow [5, 6].

Previous investigations by Williams *et al.* [7], Bratnagar and Broutman [8] and in our laboratory [9] show the presence of residual stresses in longitudinal and circumferential directions. Generally, compressive axial and circumferential components exist at the outer layers of the pipe wall. However, tensile components dominate towards the bore. It is known that the presence of these stresses is directly related to the material microstructure [6]. Consequently, the resistance of a material to crack propagation and, thus, its service lifetime will be affected by the state of stress and morphology. This paper presents results of an experiment designed to examine the influence of residual stress and associated morphology variances on the crack propagation behaviour in MDPE extruded pipes.

2. Experimental procedure

2.1. Material

The pipe material used in this investigation was supplied by Plexco Inc. (Franklin Park, Illinois, USA). The pipes were especially extruded from unpigmented (natural) resin specified as PE 2306-IIC (natural). This code designates that the material is extruded medium-density polyethylene with melt flow index in the range 0.4 to 1.5 [10]. Each pipe has a minimum wall thickness of 11.1 mm and an average outside diameter of 113.7 mm.

2.2. Specimen preparation

Rectangular strips were cut from the pipe wall. The preparation employs an assembly of two circular saws mounted on a Bridgeport milling machine (Fig. 1). Each saw is 69.85 mm diameter and 1.04 mm thick. The specimen thickness was set by appropriate spacers between the saws. Cutting was performed at the lowest speed of the machine (325 r.p.m.). Through this operation, pressurized air was used as a cooling medium to minimize possible material softening due to frictional heat generation. The specimens were cut to the dimensions 152.4 mm × 2 mm × 11.1 mm.

Two identical specimens were notched from the outer side of the pipe wall (specimen A) and the other from the inner side (specimen B). A sketch showing both specimens is presented in Fig. 2. Prior to notching, the specimens were placed in liquid nitrogen to ensure minimum damage at the notch-tip. A notching press was employed to control the notch direction as well as the notch depth (1 mm).

2.3. Loading conditions

The specimens were subjected to a constant load of 6.75 MN m^{-2} ($\sim 0.3\sigma_y$). This stress level was chosen based on the results of fatigue crack propagation experiments [11] to ensure slow propagation within a reasonable time. Some of the axial residual stresses were relieved upon preparation causing some curvature in the specimens (Fig. 2). This amount was restored by applying the appropriate bending moment to straighten the specimens before final clamping to the creep fixture. Pure Igepal CO-630, an environmental stress cracking agent supplied by General Aniline and Film Co. (GAF), was sprayed into the notch-mouth to accelerate initiation. When the cracks were 1 mm ahead of the notch-tip, no Igepal was subsequently used. Crack propagation was observed under transmitted light. The crack tip was followed at × 10 magnification. The entire experiment was conducted at ambient conditions.

0022–2461/87 $03.00 + .12

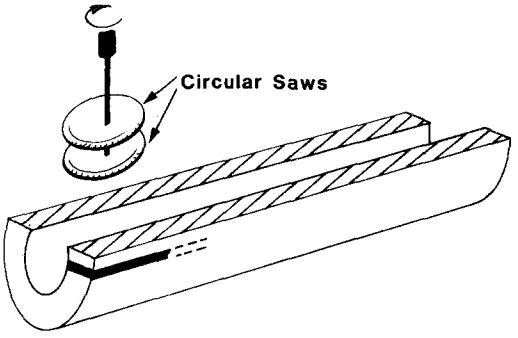

Figure 1 Double circular saw fixture used to prepare specimens.

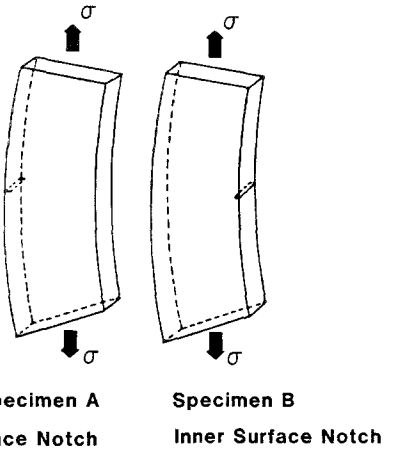

Figure 2 Sketch of specimens A and B after preparation. Relief of residual stresses causes bending as shown.

3. Results

Transmitted light micrographs showing propagating cracks in the two specimens are exhibited in Fig. 3. Both photographs were taken simultaneously 2500 h from the onset of loading. The markers beneath the cracks are 1 mm apart. Obviously, the extent of crack propagation in specimen B (outbound) is twice that of A (inbound). The arrows indicate the crack tips. In each case, the crack is preceded by a single craze-like entity resembling that noted in high-density polyethylene under creep [12] and fatigue [13] loadings. One major difference, however, is that the single craze-like damage zone remains unaltered during the entire slow crack propagation in this experiment. On the other hand, the craze-like zone in HDPE undergoes ductile transformations as the crack grows longer [12–14].

Shown in Fig. 4 is the crack propagation behaviour within the first 400 h. The crack in specimen B (outbound) took 61 h to propagate 1 mm from the notch-tip. Crack extension for the same distance (1 mm) took only 11 h in specimen A (inbound). After that, the rate of propagation in A was significantly lower than that of B. This trend continued, as shown in Fig. 5, leading to temporary crack arrest of the inbound crack after 216 h. Around 4000 h later, the arrested crack propagated from 3 to 5.5 mm to be again arrested for approximately 1200 h. Finally, the crack speed was accelerated towards failure in 7709 h. The outbound crack behaviour exhibited neither of the arrest stages. Rather, it accelerates monotonically to ultimate failure at 3705 h.

To examine the extent of Igepal influence on the fracture process, the fracture surfaces of both specimens were examined with scanning electron microscopy (SEM). Fig. 6 shows the corresponding micrographs. The area A indicates the notch region while area B characterizes the zone affected by the presence of Igepal. Tortuously yielded features [15] on the surface dominate the failure mechanisms. The post-Igepal fracture represented by area C is totally different whether considering the inbound crack (Fig. 6a) or the outbound crack (Fig. 6b). The first arrest stage shown in Fig. 5 is clearly recognizable by its oriented surface tearing marks in the direction of crack advances (Fig. 6a). Detailed fractographic analysis will be published in a subsequent paper.

4. Discussion

The markedly different inbound and outbound crack propagation behaviour in the "same material" suggests that the material's resistance to fracture is strongly influenced by its processing history. Among several factors, processing conditions involve preferential cooling and non-homogeneous melt flow. These factors introduce differences in morphology [16] and residual stresses [9].

The crack layer (CL) theory [17–20] defines the crack driving force as the difference $(G_1 - \gamma^* R_1)$, where γ^* is the specific enthalpy of damage and R_1 is the resistance moment representing the amount of damage required for crack advance. G_1 is the energy release rate due to crack propagation. Residual stress effects can be assessed by appropriate energy release rate calculations which account for the actual stress

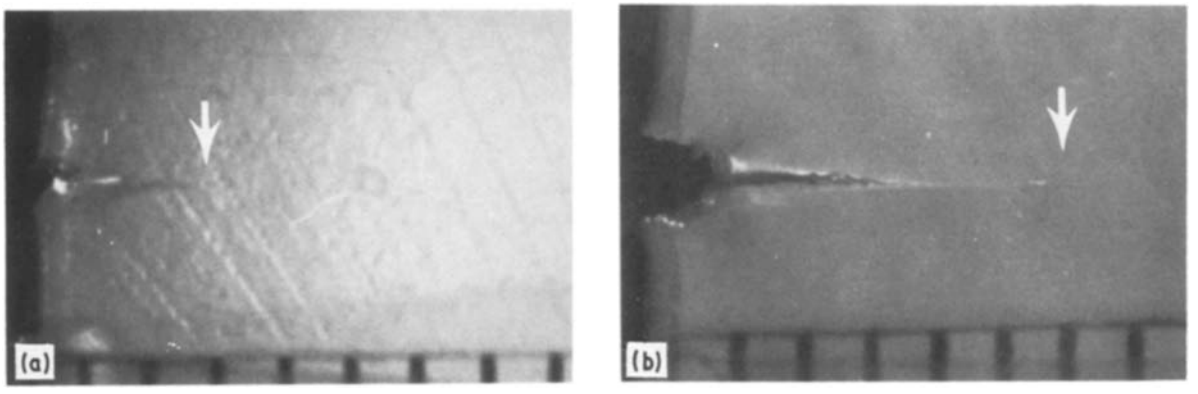

Figure 3 Optical micrographs of (a) inbound crack (A) and (b) outbound crack (B) after 2500 h. The arrows indicate crack-tips.

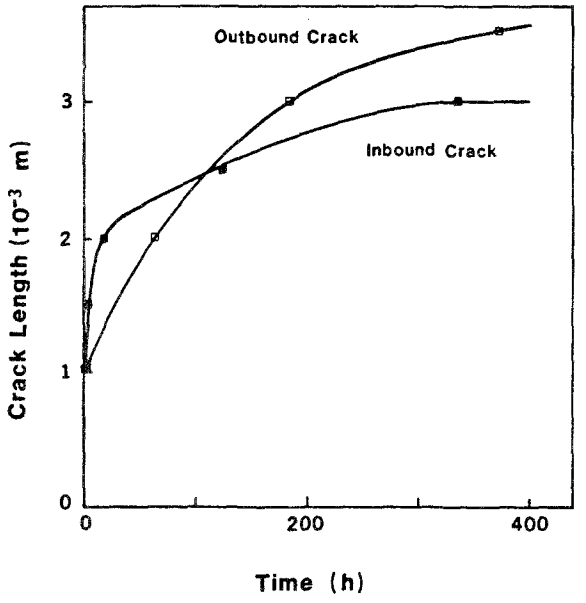

Figure 4 Comparison of inbound (A) and outbound (B) crack propagation within the first 400 h.

distribution. If this is the only dominant factor influencing the fracture process, the rate of crack propagation in both specimens should be a single function of the energy release rate so calculated. Otherwise, morphological differences reflected in $\gamma^* R_1$ ought to be responsible for the observed variance.

Hence, in this section, we discuss a method to incorporate residual stress distribution in energy release rate calculations, in terms of which we analyse the crack propagation kinetics.

4.1. Residual stresses

The test specimens were under a complex stress distribution resulting from longitudinal residual stress and the applied constant load. The longitudinal residual stress distribution (dashed curve in Fig. 7) was calculated from the circumferential component (solid curve in Fig. 7) obtained from strain gauge analysis. Details of this procedure have been reported recently [21]. The technique involves the application of strain gauges to pipe rings turned to different thicknesses, thus yielding direct measurements of the strain relieved upon cutting each ring into two halves. It is assumed that the three principal stresses have a rotational symmetry along the longitudinal direction of the cylinder [22, 23]. The results in Fig. 7 qualitatively agree with those obtained from the curvature and ring slitting methods [7, 8, 21]. Although the strain gauge technique gave rise to more realistic values, it is understood that these results are limited by factors such as viscoelastic behaviour of the material and strain gauge adhesion to PE. Obviously, the curvature of the specimen sketched in Fig. 2 is the direct consequence of the residual stress distribution. However, no attempt was made to calculate the initial curvature from this distribution.

As illustrated in Fig. 7, the longitudinal residual stress distribution exhibits high compressive components on the outer shell. The maximum value measured is $-4.5\,\mathrm{MN\,m^{-2}}$ ($\sim 20\%\ \sigma_y$). At the bore, however, the maximum tensile component averages $0.5\,\mathrm{MN\,m^{-2}}$. An interval of zero residual stress exists at about 1.5 mm from the pipe bore.

4.2. Crack propagation kinetics

The delayed crack initiation for the first millimetre of crack extension in specimen B (Fig. 4) can be attributed to combined effects of the applied load and the tensile residual stress. This results in sufficiently high stress at the notch-tip to cause blunting. This can be inferred from Fig. 6 where highly deformed features appear within the first millimetre of crack growth. Blunting leads to a lower local stress concentration and consequently a delayed crack growth. A similar argument is invoked for accelerated crack initiation from the outer pipe known to cause less blunting and hence, faster crack initiation is observed (Fig. 4).

Morphological examination of the same pipe material reveals the presence of lamellar micro-crystalline domains, the average size of which increases from the exterior to the interior of the pipe wall [16]. This morphological change could additionally contribute to the noted difference in the crack propagation behaviour. The deformation features shown in Fig. 6 lend support to the morphological effect.

4.3. Energy release rate

The residual stress noted in Fig. 7 causes non-uniformity of stress distribution along the crack

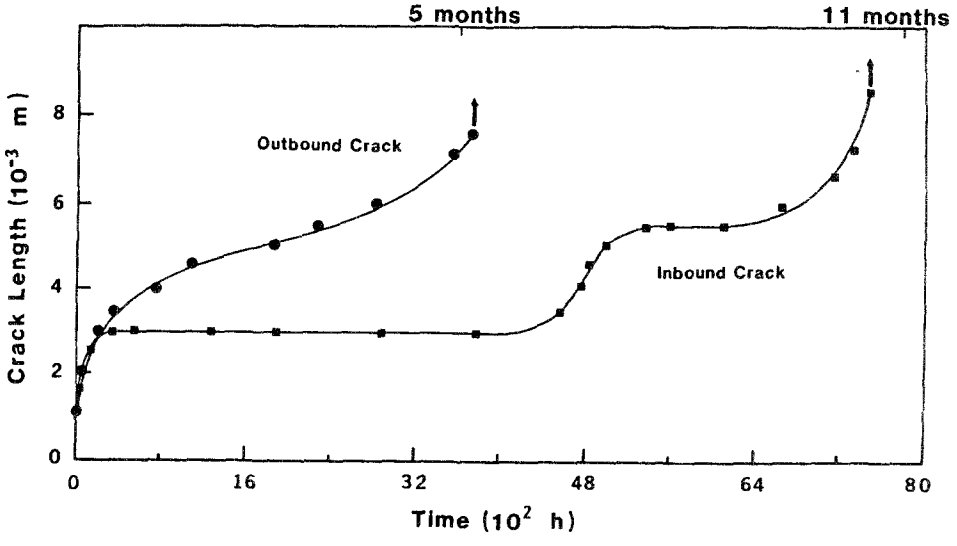

Figure 5 Overall crack propagation behaviour. Vertical arrows indicate ultimate failures.

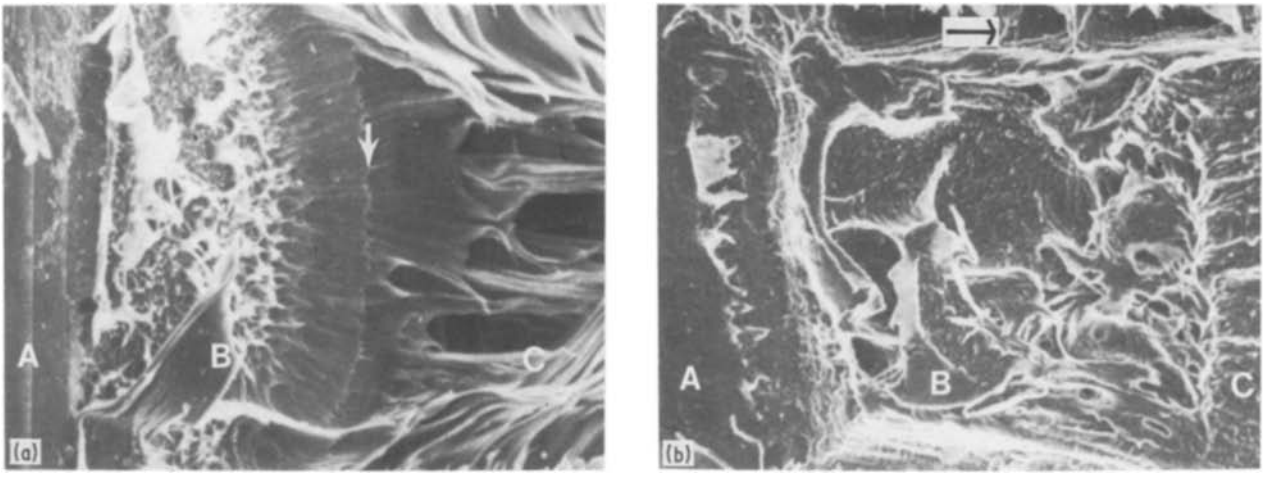

Figure 6 Scanning electron micrographs showing initiation of (a) inbound and (b) outbound cracks. Region A corresponds to the notch while B represents the zone affected by Igepal. Region C is the beginning of the propagation zone with no effect of Igepal. Vertical arrow in (a) indicates the first arrest stage in Fig. 5. The horizontal arrow indicates the crack propagation direction.

trajectory. Thus, to evaluate the stress intensity factor, K_I, we make use of the Green's function derived for a unit dipole force applied to the crack faces in opposite directions at a point x in a single edge notched (SEN) specimen [24], i.e.

$$K_I = \frac{2}{(\pi l)^{1/2}} F\left(\frac{x}{l}, \frac{l}{B}\right) \quad (1)$$

where $F(x/l, l/B)$ is given in the Appendix. Then, the resulting stress intensity factor accounting for residual stresses in the specimens considered is obtained as

$$K_I = \frac{2}{(\pi l)^{1/2}} \int_0^l P(x) F\left(\frac{x}{l}, \frac{l}{B}\right) dx \quad (2)$$

$P(x)$ is the traction distribution due to the applied and residual stresses in a cracked specimen along the line coincident with the crack path. Assuming linear elastic behaviour, the energy release rate G_I is given by

$$G_I = \frac{K_I^2}{E} \quad (3)$$

where E is the elastic modulus of the material, found to be $0.55\,\mathrm{GN\,m^{-2}}$.

Fig. 8 shows the energy release rate for each specimen plotted as a function of crack length. The energy release rate associated with the outbound crack propagation, G_I^B, is always higher than that associated with the inbound crack G_I^A. This is obviously because of the dominant tensile residual stress towards the inner pipe skin (bore). For further illustration of this difference, the ratio of G_I^A to G_I^B is plotted as a function of crack length in Fig. 9. In the initial crack growth stage (first millimetre), the energy released from the inbound crack is five times that of the outbound crack. The actual values calculated at 1 mm crack extension are $G_I^B = 0.75\,\mathrm{kJ\,m^{-2}}$ and $G_I^A = 0.15\,\mathrm{kJ\,m^{-2}}$. As each of the two cracks propagates deeper, the difference between G_I^B and G_I^A becomes smaller. The critical energy release rate of the outbound G_{Ic}^B is about $77\,\mathrm{kJ\,m^{-2}}$. The energy release rate associated with the inbound crack at the same crack length ($l_c^B = 8\,\mathrm{mm}$) is about $0.58 G_I^B$ (Fig. 9). In fact, the outbound crack exhibited a critical crack length of $l_c^A \simeq 8.5\,\mathrm{mm}$. Consequently, the outbound critical energy release rate amounts to $107\,\mathrm{kJ\,m^{-2}}$.

The crack propagation rates are plotted as a function of the energy release rate in Fig. 10. It is immedi-

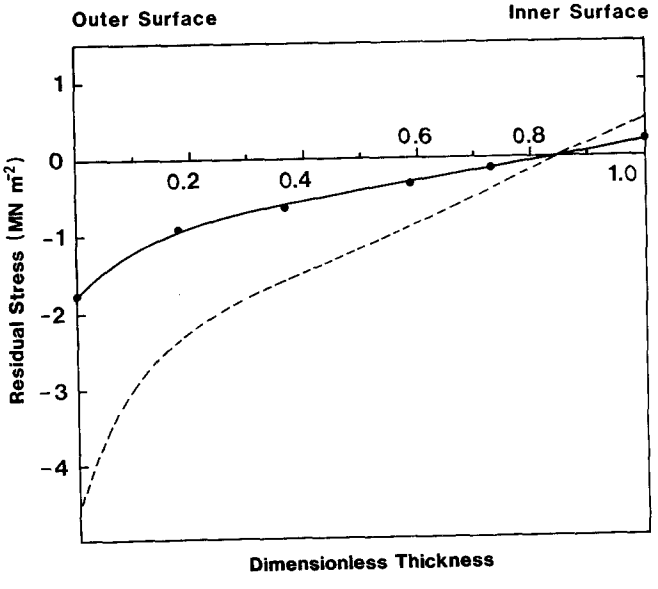

Figure 7 Distribution of the axial component (σ_{zz}) of residual stresses through the pipe wall (broken line). Solid line corresponds to the circumferential component ($\sigma_{\theta\theta}$).

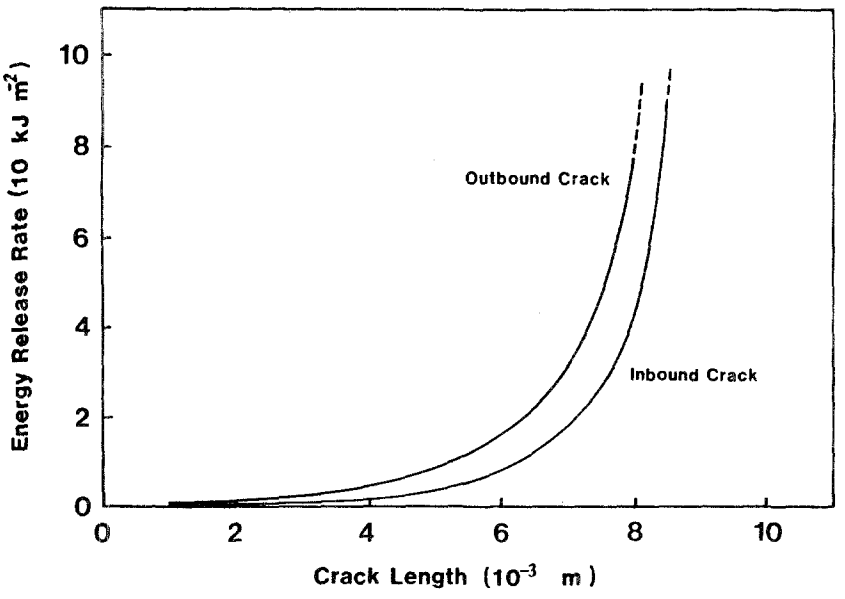

Figure 8 Energy release rates for inbound (A) and outbound (B) cracks. The difference is due to residual stresses.

ately obvious that the crack propagation behaviour in the "same material" is not a unique function of the energy release rate. The outbound crack speed decelerates to a minimum at about 10 kJ m^{-2} beyond which it accelerates to ultimate failure. The inbound crack, on the other hand, displays markedly different behaviour. It was arrested at 1.2 kJ m^{-2} for about 4000 h, resumed anomalous propagation behaviour to be arrested again at 5.8 kJ m^{-2} for almost 1200 h. The critical crack lengths in both cases were determined from fractographic analysis [11].

Apparently, the energy release rate is not a unique controlling parameter for the observed crack propagation behaviour. The fracture mechanisms at the same level of energy release rate are notably different. Fig. 11 samples the fracture surface of inbound (Fig. 11a) and outbound (Fig. 11b) cracks at an equal energy release rate of 5 kJ m^{-2}. The fracture surface in Fig. 11a displays more localized yielding than Fig. 11b. This suggests differences in the manner by which the material transforms in resistance to crack propagation. The fact that G_1, which accounts for residual stress, does not solely explain the contrasting crack propagation behaviour, suggests that differences in γ^* and/or R_1 underly this phenomenon.

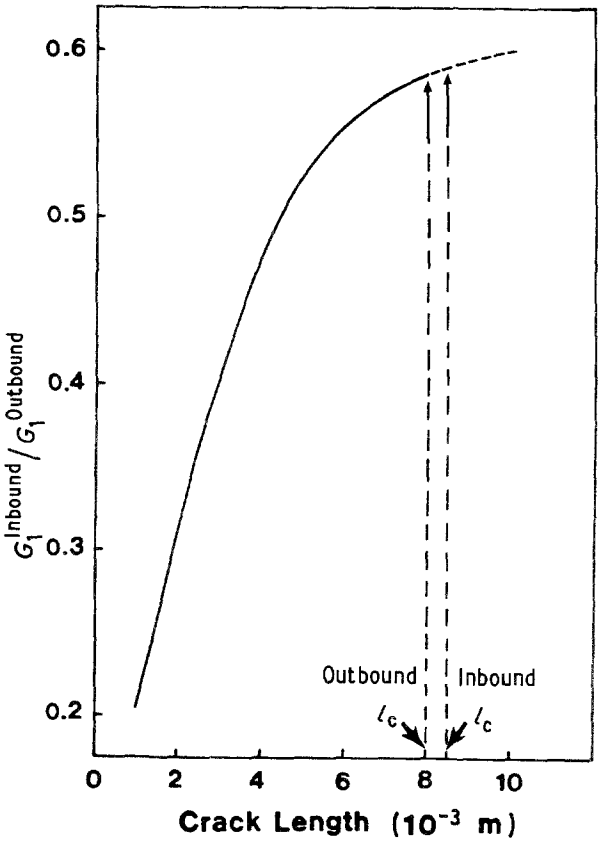

Figure 9 The ratio of G_1^A/G_1^B as a function of crack length.

5. Conclusions

1. MDPE pipes exhibit more resistance to inbound crack propagation. This behaviour is seemingly related to processing conditions which introduce residual stresses and morphological gradients.

2. A method to incorporate the residual stress distribution in energy release rate calculations is introduced.

3. The rates of inbound and outbound crack propagation do not show unique dependence on the respective energy release rate. This suggests that morphological variances across the pipe wall contribute to the material's resistance to crack propagation.

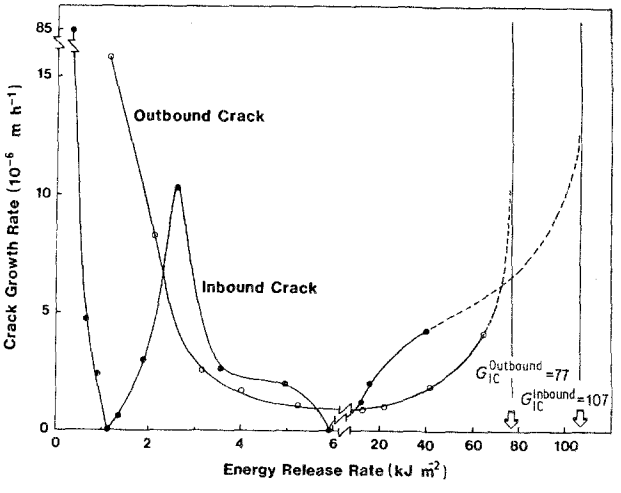

Figure 10 Crack growth rates as a function of energy release rate.

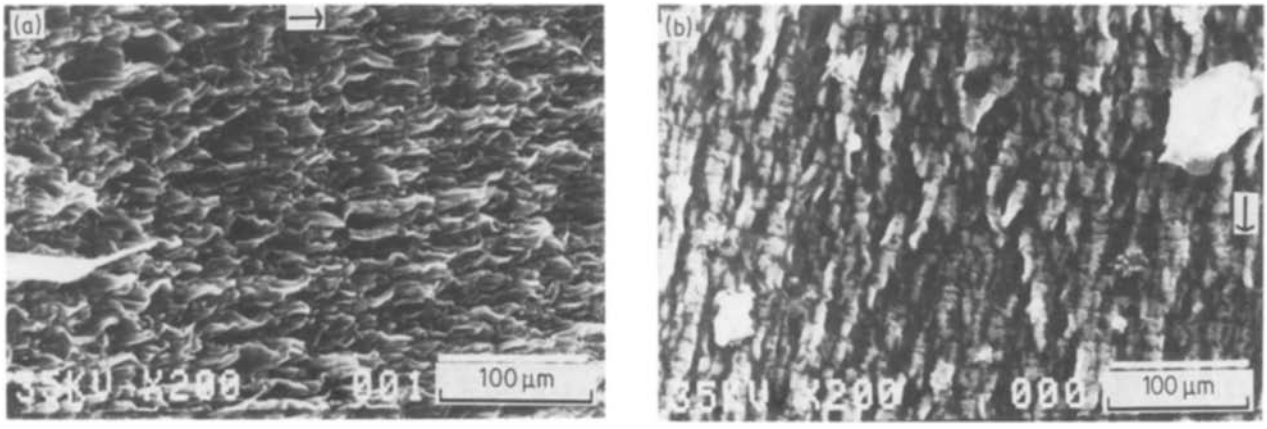

Figure 11 Scanning electron micrographs of the fracture surface for (a) inbound and (b) outbound cracks at the same energy release rate level (5 kJ m^{-2}).

Acknowledgements

The authors wish to extend their thanks to Dr P. Petro from Plexco Inc. for pipe sample preparation, Dr M. Klein for useful discussions and Professor P. H. Geil for sharing unpublished morphological results. The financial support of the Gas Research Institute under grant number 5083-260-0940 is greatly appreciated.

Appendix

For a single edge notched specimen with a known localized unit point load P, the stress intensity for factor in mode I is written as [24]

$$K_I = \frac{2}{(\pi l)^{1/2}} F\left(\frac{x}{l}, \frac{l}{B}\right) \quad \text{(A1)}$$

where l is the crack length, B is the specimen width, x is the distance from the notched edge to the point of load application (Fig. A1) and $F(x/l, l/B)$ is given by

$$F\left(\frac{x}{l}, \frac{l}{B}\right) = \frac{3.52(1 - x/l)}{(1 - x/B)^{3/2}} - \frac{4.52 - 5.28x/l}{(1 - x/B)^{1/2}} + \left\{\frac{1.30 - 0.30(x/l)^{3/2}}{[1 - (x/l)^2]^{1/2}} + 0.83 - 1.76x/l\right\} \times (1 - (1 - x/l)\, l/B) \quad \text{(A2)}$$

In the case of localized distributed load $P(x)$ along a line coincident with the crack path, Equation A1 becomes

$$K_I = \int_0^l \frac{2}{(\pi l)^{1/2}} P(x) F(x/l, l/B)\, dx \quad \text{(A3)}$$

The load levels (residual and applied) of inbound and outbound cracks are approximated by a third degree polynomial. Thus, for the inbound crack (specimen A), $P(x)$ is obtained as:

$$P(x) = 10^{-5}x^3 - 0.209x^2 + 1.664 \times 10^3 x + 0.855 \times 10^6 \quad \text{(A4)}$$

Considering Equations A2 and A4 and using $x/l = \xi$, Equation A3 can be rewritten as

$$K_I^A = \frac{2l}{(\pi l)^{1/2}} \int_0^1 \left\{\left[\frac{3.52(1 - \xi)}{(1 - l/B)^{3/2}} - \frac{4.52 - 5.28\xi}{(1 - l/B)^{1/2}} + \left(\frac{1.30 - 0.3\xi^{3/2}}{(1 - \xi^2)^{1/2}} + 0.83 - 1.76\xi\right) \times (1 - (1 - \xi)\, l/B)\right] [0.010 \times 10^{-3} l^3 \xi^3 - 0.209 l^2 \xi^3 + 1.664 l\xi + 0.855 \times 10^6]\right\} d\xi \quad \text{(A5)}$$

Similarly, K_I^B is calculated using Equation A5 into which ξ of $P(\xi)$ is replaced by $(B/l - \xi)$.

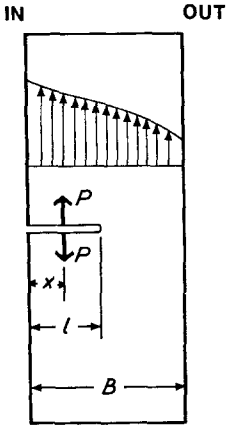

Figure A1 Sketching showing concentrated local load with respect to crack length. The vertical arrows illustrate the load level accounting for residual stress.

References

1. J. M. HODGKINSON and J. G. WILLIAMS, "Deformation Yield and Fracture of Polymers" (1983) p. 35.1.
2. J. F. MANDELL, K. L. SMITH and D. D. HUANG, *Polym. Engng Sci.* **21** (1981) 1173.
3. G. J. SANDILANDS and J. R. WHITE, *Polymer* **21** (1980) 338.
4. M. R. KAMAL and V. TAN, *Polym. Engng Sci.* **19** (1979) 558.
5. C. S. BARRETT, "Experimental Stress Analysis", Proceedings of the Society for Experimental Stress Analysis, Vol. II, no. I (1944) 147.
6. L. C. E. STRUIK, *Polym. Engng Sci.* **18** (1978) 799.
7. J. G. WILLIAMS, J. M. HODGKINSON and A. GRAY, *ibid.* **21** (1981) 822.
8. A. BRATNAGAR and L. J. BROUTMAN, *SPE Antec '85* (1985) 545.
9. K. CHAOUI, Master's Thesis, Case Western Reserve University (1986).

10. ASTM D 3350-83, "Annual Book of ASTM Standards", Vol. 08.04, Plastic Pipe and Building Products (1984).
11. K. CHAOUI, A. MOET and A. CHUDNOVSKY, to be published.
12. N. BROWN and S. K. BHATTACHARYA, *J. Mater. Sci.* **20** (1985) 4553.
13. K. SEHANOBISH, A. CHUDNOVSKY and A. MOET, *Polymer*, in press
14. K. CHAOUI, M. L. KASAKEVICH, K. SEHANOBISH, A. CHUDNOVSKY and A. MOET, GRI Annual Report (1986).
15. S. BANDYOPADHYAY and H. R. BROWN, *Polym. Engng Sci.* **20** (1980) 720.
16. P. H. GEIL, personal communications.
17. A. CHUDNOVSKY, "Crack Layer Theory", NASA Report, CR-174634 (1984).
18. A. CHUDNOVSKY and A. MOET, *J. Mater. Sci.* **20** (1985) 630.
19. *Idem, J. Elastomers Plastics* **18** (1986) 50.
20. N. HADDAOUI, A. CHUDNOVSKY and A. MOET, *Polymer* **27** (1986) 1377.
21. K. CHAOUI, A. CHUDNOVSKY and A. MOET, *J. Testing Eval.* (1986) in press.
22. V. G. SACHS, *Z. Metallkde* **19** (1927) 352.
23. V. G. SACHS and G. ESPEY, *Iron Age* **148** (1941).
24. H. TADA, P. C. PARIS and G. P. IRWIN, "The Stress Analysis Handbook" (Del. Research Corporation, Helertown, Pennsylvania, 1973).

Received 18 September 1986
and accepted 4 March 1987